ISSN 1070-3284, Russian Journal of Coordination Chemistry, 2017, Vol. 43, No. 4, pp. 206–212. © Pleiades Publishing, Ltd., 2017.
Original Russian Text © V.A. Grinberg, N.A. Maiorova, A.A. Pasynskii, V.V. Emets, A.A. Shiryaev, V.V. Vysotskii, V.K. Gerasimov, V.V. Matveev, E.A. Nizhnikovskii, V.N. Andreev, 2017, published in Koordinatsionnaya Khimiya, 2017, Vol. 43, No. 4, pp. 204–211.

Nanostructured Catalysts for Direct Electrooxidation of Dimethyl Ether Based on Bi- and Trimetallic Pt–Ru and Pt–Ru–Pd Alloys Prepared from Coordination Compounds

V. A. Grinberg[a], *, N. A. Maiorova[a], A. A. Pasynskii[b], **, V. V. Emets[a], A. A. Shiryaev[a], V. V. Vysotskii[a], V. K. Gerasimov[a], V. V. Matveev[a], E. A. Nizhnikovskii[a], and V. N. Andreev[a]

[a] *Frumkin Institute of Physical Chemistry and Electrochemistry, Russian Academy of Sciences, Moscow, 117071 Russia*
[b] *Kurnakov Institute of General and Inorganic Chemistry, Russian Academy of Sciences, Moscow, 117907 Russia*
**e-mail: vgrinberg@phyche.ac.ru*
***e-mail: aapas@gmail.com*

Received July 12, 2016

Abstract—Bi- and trimetallic platinum–ruthenium and platinum–ruthenium–palladium catalysts with specified atomic ratios Pt : Ru = 1 : 1 and Pt : Ru : Pd = 1 : 1 : 0.1, respectively, were synthesized from the coordination compounds of the metals deposited on highly dispersed carbon black. The catalysts were characterized by powder X-ray diffraction, electron dispersive analysis, and transmission electron microscopy. According to voltammetry data, the highest activity in the dimethyl ether (DME) electrooxidation is exhibited by the catalyst $Pt_{0.43}Ru_{0.47}Pd_{0.1}/C$; hence, it may be considered as a promising anode material for direct DME fuel cells.

Keywords: nanoelectrocatalysts, specific activity, dimethyl ether electrooxidation
DOI: 10.1134/S1070328417040017

INTRODUCTION

In recent years, the major attention of researchers has been attracted by fuel cells involving direct methanol electrooxidation (Direct Methanol Fuel Cells, DMFC), which are considered to be most appropriate for portable devices owing to high energy density and the ease of methanol storage as compared with hydrogen. Nevertheless, the productivity of DMFC is restricted by a number of factors, the major ones being the insufficient oxidation rate and methanol crossover through the polymeric electrolyte membrane [1]. Dimethyl ether (DME), which is a less toxic fuel than methanol, came to the attention in the last decade as a possible alternative for direct oxidation fuel cells [2–7]. The open circuit voltage (OCV) of a direct DME fuel cell (DDMEFC) is comparable to that of DMFC (1.18 vs. 1.21 V) [8]. Theoretically, DME can be oxidized to carbon dioxide with participation of 12 electrons, which would provide higher energy density in the case of DME than with methanol (8.2 vs. 6.1 kW h kg^{-1}) [9]:

$$CH_3OCH_3 + 3H_2O \rightarrow 2CO_2 + 12H^+ + 12e^-. \quad (1)$$

The lower dipole moment of the DME molecule may result in a lower crossover compared with that of methanol; this would reduce the energy loss caused by the establishment of mixed potential at the opposing electrode [10, 11]. Unlike direct methanol, ethanol, and formic acid fuel cells, direct DME fuel cells have been poorly elaborated. The mechanism of DME oxidation has not yet been adequately studied, and the catalysts suitable as anode materials for DDMEFC are still to be developed.

Relying on the IR spectroscopic data, it was suggested [12] that, like in the case of methanol, chemisorbed carbon monoxide is the predominant species in the DME oxidation on Pt at low potentials [12]. Therefore, bimetallic catalysts based on Pt alloys (e.g., PtRu), which efficiently oxidize the adsorbed CO species, could also be suitable for DME oxidation [13]. Indeed, PtRu-based catalysts have been recognized in [14] to be most active for DME electrooxidation, whereas according to [8], the oxidation of DME on the PtRu catalyst is less efficient than methanol oxidation. According to the mechanism of Pt-catalyzed DME oxidation proposed in [10, 15], slow DME oxidation kinetics can be accounted for by the high activation barrier for C–O bond cleavage:

$$CH_3OCH_3 + Pt \rightarrow Pt(C{-}O{-}CH_3)_{ads} + 3e^- + 3H^+, \quad (2)$$

$$Pt(C{-}O{-}CH_3)_{ads} + H_2O \rightarrow Pt(HCO)_{ads} + CH_3OH, \quad (3)$$

$$Pt(HCO)_{ads} \rightarrow Pt(CO)_{ads} + H^+ + e^-, \quad (4)$$

$$Pt(HCO)_{ads} + Pt{-}OH \rightarrow 2Pt + CO_2 + 2H^+ + 2e^-, \quad (5)$$

$$Pt(CO)_{ads} + Pt{-}OH \rightarrow 2Pt + CO_2 + H^+ + e^-. \quad (6)$$

According to the data of [16], cleavage of esters is accelerated in the presence of palladium; therefore, addition of palladium to the PtRu catalyst may enhance the catalyst activity towards DME oxidation. Exactly this effect was observed in [17] upon the addition of 10% palladium to the PtRu(1 : 1)/C catalyst.

The results of studies of the catalytic activity of highly dispersed PtRu alloy particles for the preparation of efficient anode catalysts are extensively presented in [18–24]. The factors considered to affect the activity of these alloys supported on carbon include their composition [19, 25], uniformity of distribution on the support surface [25], the metal particles morphology and size [26], their electronic state [27–29], the presence of impurities, and the properties of the carbon supports [30–32]. A new approach to the synthesis of catalytic systems for fuel cells was developed in [33–35], using heterometallic clusters in which platinum and other metal atoms surrounded by organic groups occur in a strict stoichiometric ratio and are linked either directly or through bridging groups. For instance, Adams et al. demonstrated that the bimetallic Pt–Ru catalyst obtained from the $Pt_2Ru_4(CO)_{18}$ cluster complex is 5 times more active towards methanol oxidation than the commercial PtRu/C E-TEK catalyst, with twice lower amount of platinum in the former [34]. Bimetallic cluster precursors for the formation of Pd-Mo-P nanoparticles were described in [35]; simultaneously it was shown that mesoporous support materials are preferred for the formation of uniform nanoparticles.

Here we developed an approach to the synthesis of bi- and trimetallic electrocatalysts based on individual Pt clusters and Ru and Pd coordination compounds, which were subjected to thermal destruction on highly dispersed carbon supports, and studied their electrocatalytic activity towards DME oxidation. Previously, it was shown that a distinctive feature of the catalysts synthesized on the basis of coordination compounds is the composition reproducibility and the uniformity of metal particle distribution over the carbon support, which ensures the stability and reproducibility of catalyst characteristics [36–42].

EXPERIMENTAL

Preparation of platinum, platinum–ruthenium, and platinum–ruthenium–palladium catalysts on the Vulcan XC-72 carbon blac*k* (specific surface area of 300 $m^2\ g^{-1}$; atomic ratios Pt : Ru = 1 : 1 and Pt : Ru : Pd = 1 : 1 : 0.1; metal : carbon black weight ratio of 30 : 70). As the initial platinum compound for the preparation of the heterometallic organic precursor, we chose ethoxydicyclopentadienyl-platinum ethoxide $(C_{10}H_{12}OC_2H_5)_2Pt_3(OC_2H_5)_4$. The ruthenium and palladium coordination complexes, $(CH_3)_3C_7H_5RuCl_2$ (ruthenium cymene dichloride) and $(\alpha\text{-}CH_3C_5H_4N)_2Pd(OOCCMe_3)_2$, respectively, served as its partners. For the catalyst preparation, highly dispersed Vulcan XC-72 carbon black was first ultrasonicated in dichloromethane, and then the required mixed solutions of precursors in dichloromethane were added dropwise; this was followed by one more ultrasonication and drying in vacuum at 100°C; the solid residue was heated in a quartz tube at 500°C under hydrogen for 45 min. After cooling and evacuation for removal of hydrogen to be replaced by high-purity argon, the catalysts thus formed contained 30 wt % metal and 70 wt % carbon black. The metal atomic ratio in the binary systems was close to 1 : 1 and the ratio of the metals in the ternary system was ~1 : 1 : 0.1.

Study of the geometric parameters of the structure and chemical microanalysis of the catalysts were performed using a scanning electron microscope (SEM) with a Quanta 650 FEG field cathode (FEI, Netherlands). Powder X-ray diffraction (PXD) analysis was carried out on an Empyrean (Panalytical) diffractometer with filtered CuK_α radiation. The standard Bragg–Brentano (reflection) geometry was used. The samples were examined without binders.

The average particle size and size distribution were determined by transmission electron microscopy (TEM) on a Philips EM-301 instrument at an accelerating voltage of 80 kV.

Electrochemical measurements. Electrochemical measurements were carried out in a standard three-electrode glass cell. A graphite disc (S = 0.636 cm^2) served as the working electrode; prior to deposition of the dispersed catalyst layer, the electrode was polished and washed with a hot alkali solution and water. The procedure of catalyst deposition on the electrode was described in detail in [41, 42]. The total metal content on the electrode was 24 μg. A platinum grid with an area of ~10 cm^2 served as the auxiliary electrode and Hg/Hg_2SO_4/0.5 M H_2SO_4 was the reference electrode. A 0.5 M solution of H_2SO_4 saturated with DME under atmospheric pressure was used as a working electrolyte. The electrolyte was prepared using a special purity grade sulfuric acid, doubly distilled water, and cylinder-stored DME. All measurements were carried out at room temperature. The potentials are referred to a hydrogen electrode in the same solution.

Since long-term cycling of the binary and ternary catalyst samples in the anodic potential region resulted in decreasing contents of the ruthenium and palladium components (because of the very low catalyst amount on the electrode), the working electrode with the deposited catalyst was first subjected to no more than 3-5 short potential pulses in the 0.05–1.0 V range for purification and surface stabilization; then voltammetric curves were recorded at a 0.002 $V\ s^{-1}$ rate in the potential range from 0.05 or 0.25 to 1.0 V. The steady-state DME oxidation currents under conditions close to the operation conditions of fuel cell anodes were

estimated by measuring the current transients at a working electrode potential of 0.5 V. The electrochemically active surface (EAS) area of the supported catalysts was determined by measuring hydrogen adsorption–desorption in the potential range of 0.05–0.4 V [43]. The true catalyst surface area was calculated from the particle size (according to TEM data).

All electrochemical measurements were carried out using an EL-02.06 automatic potentiostat coupled to a PC. The experimental data were treated using standard software.

The activity towards DME oxidation was determined for samples of nanostructured platinum, platinum–ruthenium, and platinum–ruthenium–palladium catalysts, Pt/C, PtRu (1 : 1)/C, and PtRuPd (1 : 1 : 0.1)/C, prepared by the above-described procedure with a total metal content of 30% in each of the catalysts.

RESULTS AND DISCUSSION

According to electron dispersive (EDX) analysis (typical spectra are shown in Figs. 1a, 1b), the metal atomic ratio in the prepared bimetallic Pt : Ru (1 : 1)/C catalyst varied in the range 1 : (1.09–1.47) from one surface point to another; this corresponds to the average composition given by $Pt_{0.45}Ru_{0.55}$. In the trimetallic Pt : Ru : Pd (1 : 1 : 0.1)/C catalyst, the atomic ratio of the components varied as 1 : (1.04–1.47) : 0.1, which corresponds, on average, to $Pt_{0.43}Ru_{0.47}Pd_{0.1}$ (see table below). Both catalysts showed somewhat exceeded atomic content of ruthenium. Apart from sites with decreased platinum content, there were surface sites in which the platinum content virtually coincided with the atomic ratio specified by the synthesis. This variation of the relative contents of the major components in the catalyst surface layer is probably due to their mutual diffusion during the preparation. According to laser mass spectrometry data (EMAL-2 instrument with photographic recording of ions, sensitivity of 10^{-4}–10^{-5} at %), the overall composition of the catalysts corresponded to the atomic ratios Pt : Ru = 1 : 1 and Pt : Ru : Pd = 1 : 1 : 0.1, which virtually coincided with the component ratio specified in the synthesis. A similar enrichment of the surface layer with a less noble component was observed previously for alloys dispersed on carbon black [40].

The X-ray diffraction patterns of the Pt/C, $Pt_{0.45}Ru_{0.55}$/C, and $Pt_{0.43}Ru_{0.47}Pd_{0.1}$/C catalysts are presented in Fig. 2. Apart from the weak peak from the disordered carbon support (26°), reflections from platinum and its compounds are present. All three catalysts have a face centered cubic (fcc) crystal lattice with diffraction peaks at about 39.74°, 46.32°, and 67.61° for 111, 200, and 220 reflections, respectively. The PtRuPd ternary system is characterized by broad solid solution regions; and the compositions we studied fall into the single-phase region [44]. The formation of a solid solution in the $Pt_{0.43}Ru_{0.47}Pd_{0.1}$/C catalyst is supported by the shift of the 111 peak relative to that of pure Pt. Furthermore, this reflection of $Pt_{0.43}Ru_{0.47}Pd_{0.1}$/C is somewhat shifted to lower 2θ relative to that of $Pt_{0.45}Ru_{0.55}$/C; this is apparently caused by the smaller Pd atomic radius compared with the Ru one (r_{Pt} = 1.36, r_{Ru} = 1.46, r_{Pd} = 1.39 Å) [45].

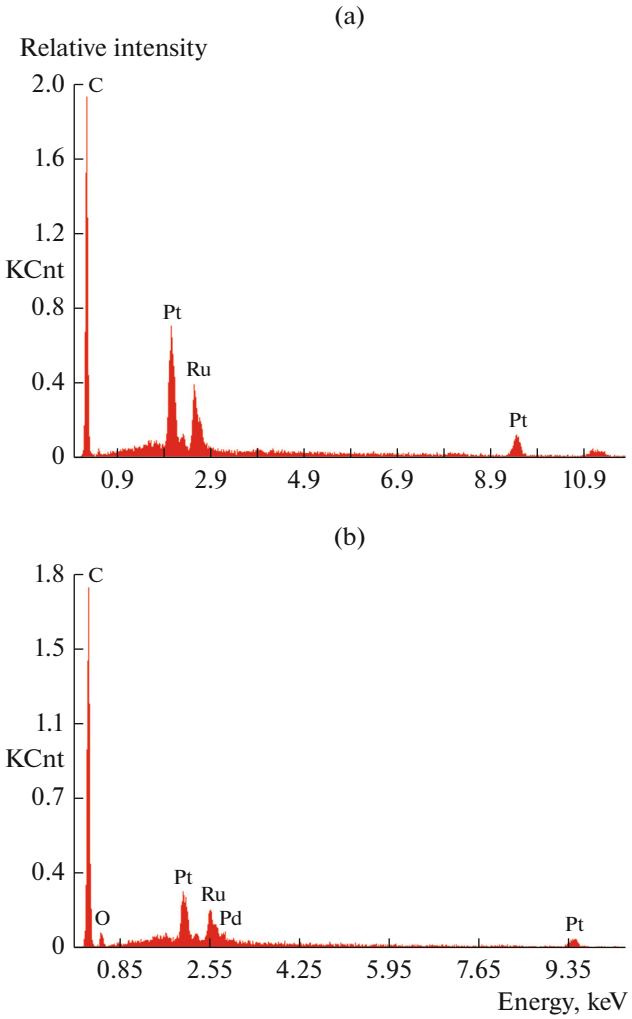

Fig. 1. Typical EDX spectra of (a) PtRu/C and (b) PtRuPd/C catalysts.

Composition of the prepared catalysts

Catalyst	Component	wt %	at %
PtRu/C	Pt	17.21	1.43
	Ru	10.96	1.75
PtRuPd/C	Pt	10.58	0.82
	Ru	6.23	0.91
	Pd	1.37	0.19

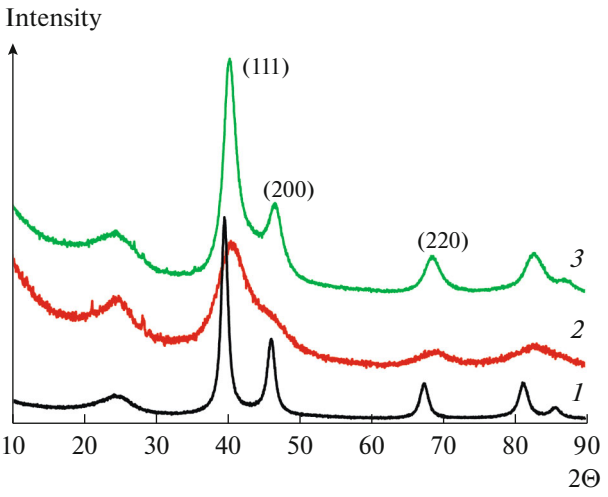

Fig. 2. XRD patterns of catalyst samples: (*1*) Pt/C, (*2*) PtRu/C; (*3*) PtRuPd/C.

The measured lattice spacing (~0.226 nm) corresponds to the (111) plane of the PtRuPd alloy. This value is between the lattice spacings for the (111) planes of Pt (0.228 nm) and the PtRu alloy (0.223 nm) [46], which confirms the incorporation of Pd into the PtRu crystal lattice. The coherent scattering regions (estimated by the Debye–Sherrer formula for different crystallographic directions and by the Williamson–Hall formula) are 7 nm for platinum, 1.6–2.2 nm for PtRu, and 3.5–4.5 nm for PtRuPd. The absence of reflections for ruthenium metal indicates that no separate ordered Ru phase is present; however, most likely, ruthenium forms a solid solution with platinum, resulting in the displacement of the principal Pt reflections and considerable decrease in size of the coherent in the coherent scattering region. A similar behavior was noted in our earlier studies for PtRu particles prepared by different methods [47, 48].

The TEM images of $Pt_{0.43}Ru_{0.47}Pd_{0.1}/C$ and $Pt_{0.45}Ru_{0.55}/C$ presented below (Figs. 3b, 3c) indicate that the morphology of both catalysts is identical and the PtRuPd and PtRu particles are uniformly distributed throughout the carbon support. The particle size distribution is rather narrow; the average particle sizes of PtRuPd and PtRu (~2.2 and 3.0 nm, respectively) are in good agreement with the crystallite size calculated from powder X-ray diffraction data.

Figure 3, which illustrate TEM data, shows the photomicrographs and particle size distribution histograms for platinum, platinum–ruthenium, and platinum–ruthenium–palladium catalysts. The particle size for the Pt/C catalyst is, on average, 2.2 nm; some particles are in the 4 to 6 nm range. In the PtRu/C catalyst, the average particle size is 3 nm and larger particles of 4 to 6.5 nm are also present. The PtRuPd/C catalyst has an average particle size of 2.2 nm and there are up to 4.2 nm particles. It is noteworthy that whereas the solid solutions show good agreement between X-ray diffraction and microscopic data, in the case of Pt/C sample, the discrepancy is significant. A possible cause is that the X-ray diffraction pattern is determined in this case by the presence of rather crystallographically perfect particles, the number of which is too small to obtain a representative statistics in analysis of TEM images.

Cyclic voltammograms measured in a 0.5 M solution of H_2SO_4 saturated with DME at room temperature and atmospheric pressure for the Pt/C, PtRu/C, and PtRuPd/C catalyst samples are shown in Fig. 4. Note that the plots shown in this and subsequent figures were obtained after subtracting the currents measured in blank experiments, i.e., without DME. It can be seen in Fig. 4 that a shift of the electrode potential to more positive values (anodic branch of the voltammogram) gives rise to a broad DME oxidation peak for all catalyst samples, the oxidation current decreasing at potentials more positive than 0.8–0.9 V; this is related to the onset of platinum surface oxidation and, hence, decreasing accessibility of the platinum surface for DME molecules being oxidized. The reduction of surface oxides restores the catalyst surface accessibility, and a DME oxidation peak is also present in the cathodic branch of the voltammogram. The potential at which DME oxidation starts depends on the catalyst composition and shifts to less positive values in the sequence Pt/C > PtRu/C > PtRuPd/C. Thus, the introduction of a minor amount of palladium into the platinum–ruthenium catalyst increases the catalyst activity towards DME oxidation, which is in line with the data of Li et al. [17].

In order to elucidate the mechanism of DME oxidation in the presence of the given catalysts, experiments on the anodic oxidation of the particles formed on the surface upon DME adsorption were carried out. For this purpose, the electrode with a deposited catalyst sample was kept at a potential of 0.25 V in a DME-saturated solution for 20 min (DME adsorption), then the solution was purged with argon for 30 min (to remove DME), and then a cyclic voltammogram was measured from the adsorption potential to 1.0 V. The results obtained for the three catalysts are presented in Fig. 5a (first cycle). It can be seen that the oxidation of adsorbed DME follows the same pattern as the DME oxidation in solution, in particular, the onset of oxidation on PtRu/C and PtRuPd/C shifts to less positive potentials relative to that for the monoplatinum catalyst. It is noteworthy, however, that whereas ~75% of the adsorbed species are oxidized during the first cycle on Pt/C and PtRu/C, this value is not more than 50% for PtRuPd/C. Presumably, the oxidation on this catalyst is accompanied by the formation of intermediates that resist oxidation. Apparently, formaldehyde may act as this intermediate of DME electrooxidation, as it can form oligomerization or polymerization products on the electrode surface and thus inhibit the oxidation of DME.

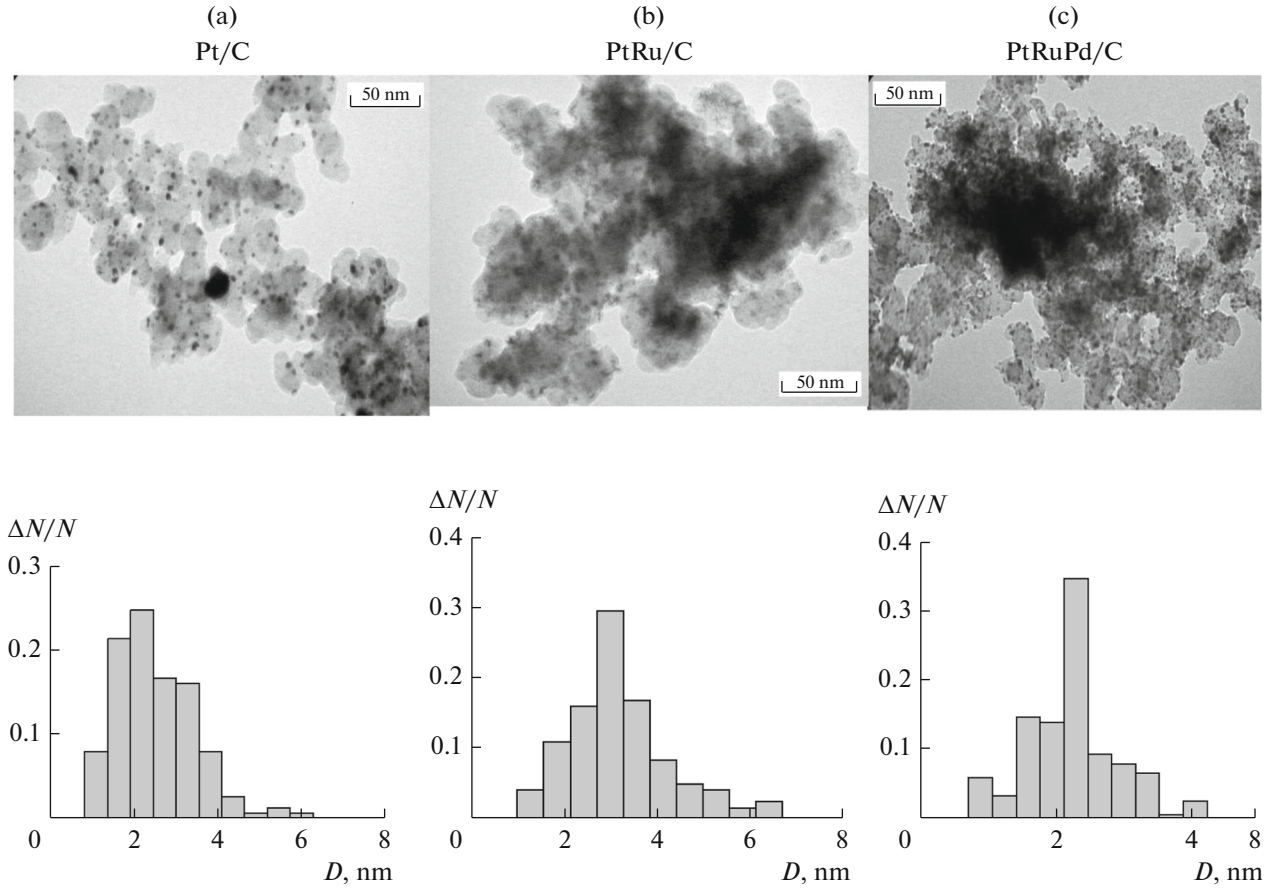

Fig. 3. Photomicrographs and particle size distribution histograms for (a) Pt/C, (b) PtRu/C, and (c) PtRuPd/C catalyst samples.

The results of experiment on the anodic oxidation of adsorbed CO species (according to the generally accepted view on the mechanisms of oxidation of DME and some other organic compounds, these species are the major chemisorption products) are illustrated in Fig. 5b. The procedure was similar to that used in DME experiments. In this case, too, the potential at which CO_{ads} oxidation started on PtRu/C or PtRuPd/C shifted to less positive values relative to that for Pt/C. The introduction of 10% palladium seems not to improve the kinetics of CO oxidation on the platinum–ruthenium catalyst (the potential at which the oxidation starts virtually does not change). Meanwhile, the charge spent for the oxidation of CO_{ads} is much greater for PtRuPd/C than for PtRu/C. A similar phenomenon was observed in [17] and attributed to higher coverage of the PtRuPd/C surface by CO_{ads} species and more efficient C–O bond cleavage in the presence of palladium. Despite the difficulty of removal of adsorbed species from the catalyst surface, the activating effect of palladium on the C–O and C–H bond cleavage is beneficial for the resultant rate of DME oxidation; this is confirmed by experiments on steady-state DME oxidation (Fig. 6).

Figure 6a shows the variation of the DME oxidation current with time for the three catalysts at an electrode potential of 0.5 V. Whereas no oxidation current is observed on Pt/C at this potential, in the case of PtRu/C and PtRuPd/C, the current densities reach 20 and 25 μA cm^{-2}, respectively.

A similar dependence for specific currents (normalized to the content of platinum as the most expensive component of the catalyst) is shown in Fig. 6b. The specific current of DME oxidation catalyzed by PtRuPd/C reaches 1.2–1.25 mA mg_{Pt}^{-1}; thus, this catalyst may be promising for the use in direct DME fuel cells.

Thus, we synthesized bi- and trimetallic platinum–ruthenium and platinum–ruthenium–palladium nanoelectrocatalysts supported on highly dispersed Vulcan XC-72 carbon black with a specified metal ratio from coordination compounds of these metals. The physicochemical characteristics and the structure of the catalysts were studied. The specific surface areas calculated from TEM data are 117 and 156 m^2/g for PtRu/C and PtRuPd/C, respectively, which is not inferior to these values for commercial catalysts. Dimethyl ether electrooxidation on PtRu/C and

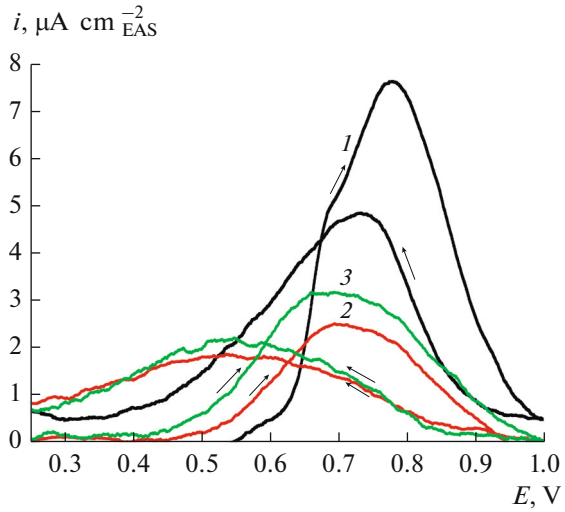

Fig. 4. Cyclic voltammograms for DME oxidation from a saturated solution catalyzed by: (*1*) Pt/C; (*2*) PtRu/C; (*3*) PtRuPd/C. Supporting solution: 0.5 M H_2SO_4. Potential sweep rate: 2 mV s^{-1}.

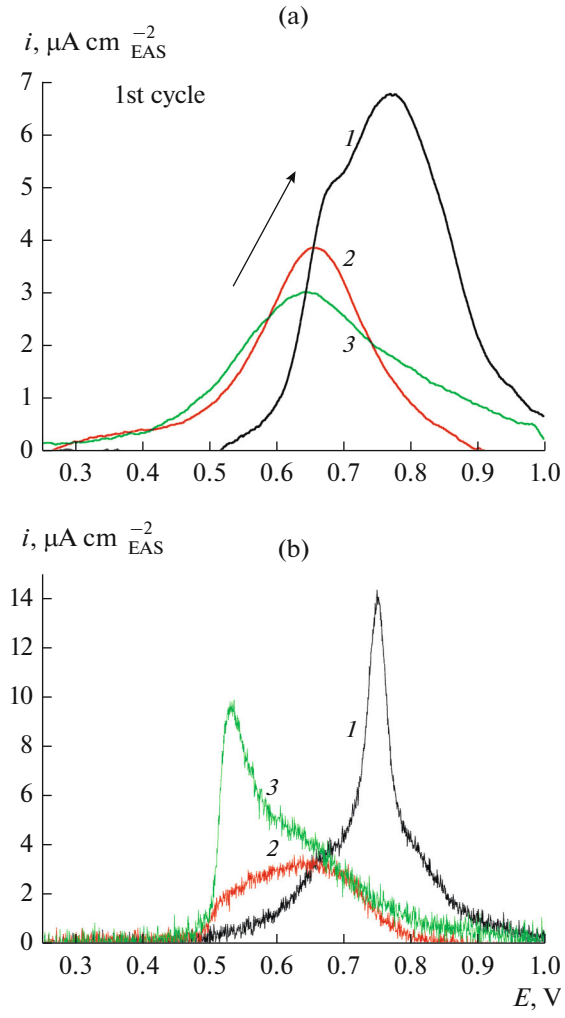

Fig. 5. Voltammograms of the anodic oxidation of adsorbed (a) DME and (b) CO at 0.25 V catalyzed by: (*1*) Pt/C; (*2*) PtRu/C; (*3*) PtRuPd/C. Potential sweep rate: 2 mV s^{-1}.

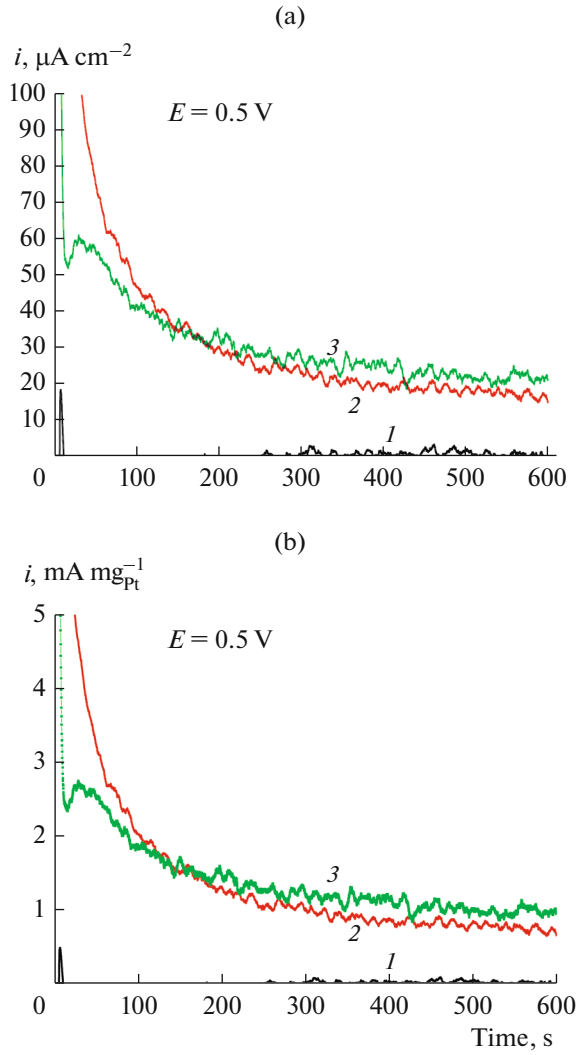

Fig. 6. (a) Current densities and (b) specific currents of DME oxidation from a saturated solution at an electrode potential of 0.5 V catalyzed by: (*1*) Pt/C; (2) PtRu/C; (*3*) PtRuPd/C. Supporting solution: 0.5 M H_2SO_4.

PtRuPd/C at room temperature was studied. It was demonstrated that the PtRuPd/C catalyst surpasses bimetallic PtRu/C systems in the specific catalytic activity and can be considered as a promising anode material for DDMEFC.

ACKNOWLEDGMENTS

X-ray diffraction studies and SEM examination combined with X-ray microanalysis of the surface layer were accomplished using the equipment of the Center for Collective Use of Physical Investigation Methods of the Frumkin Institute of Physical Chemistry and Electrochemistry, Russian Academy of Sciences.

This work was supported by the Russian Foundation for Basic Research, project nos. 16-29-09368 and 16-03-00798.

REFERENCES

1. Ahmed, M. and Dincer, I., *Int. J. Energy Res.*, 2011, vol. 35, p. 1213.
2. Müller, J.T., Urban, P.M., Holderich, W.F., et al., *J. Electrochem. Soc.*, 2001, vol. 147, p. 4058.
3. Jensen, J.O., Vassiliev, A., Olsen, M.I., et al., *J. Power Sources*, 2012, vol. 211, p. 173.
4. Im, J.Y., Kim, B.S., Choi, H.G., and Cho, S.M., *J. Power Sources*, 2008, vol. 179, p. 301.
5. Ueda, S., Eguchi, M., Uno, K., et al., *Solid State Ionics*, 2006, vol. 177, p. 2175.
6. Yu, J.H., Choi, H.G., and Cho, S.M., *Electrochem. Commun.*, 2005, vol. 7, p. 1385.
7. Kerangueven, G., Coutanceau, C., Sibert, E., et al., *J. Power Sources*, 2006, vol. 157, p. 318.
8. Li, Q., Wu, G., Johnston, C.M., and Zelenay, P., *Electrocatalysis*, 2014, vol. 5, no. p. 310.
9. Li, Q., Wu, G., Bi, X.Z., et al., *ECS Trans.*, 2013, vol. 50, p. 1933.
10. Lamy, C., Léger, J.-M., and Srinivasan, S., *Modern Aspects* of *Electrochemistry*, Bockris, J. O'M. and Conway, B.E., Eds, New York: Plenum, 2000.
11. Mizutani, I., Liu, Y., Mitsushima, S., et al., *J. Power Sources*, 2006, vol. 156, p. 183.
12. Liu, Y., Muraoka, M., Mitsushima, S., et al., *Electrochim. Acta*, 2007, vol. 52, p. 5781.
13. Liu, Y., Mitsushima, S., Ota, K., and Kamiya, N., *Electrochim. Acta*, 2006, vol. 51, p. 6503.
14. Serov, A. and Kwak, C., *Appl. Catal. B*, 2009, vol. 91, p. 1.
15. Votchenko, E.Y., Kubanova, M.S., Smirnova, N.V., and Petrii, O.A., *Russ. J. Electrochem.*, 2010, vol. 46, p. 212.
16. Widenhoefer, R.A., Zhong, H.A., and Buchwald, S.L., *J. Am. Chem. Soc.*, 1997, vol. 119, p. 6787.
17. Li, Q., Wen, X., Wu, G., et al., *Angew. Chem.*, 2015, vol. 127, p. 7634.
18. Bockris, J.O. and Wroblowa, H., *J. Electroanal. Chem.*, 1964, vol. 7, p. 428.
19. Watanabe, M. and Motoo, M., *J. Electroanal. Chem.*, 1975, vol. 60, p. 267.
20. McNicol, B.D. and Short, R.T., *J. Electroanal. Chem.*, 1977, vol. 81, p. 249.
21. Goodenough, J.B., Hamnett, A., Kennedy, B.J., et al., *J. Electroanal. Chem.*, 1988, vol. 240, p. 133.
22. Hamnett, A., Weeks, S.A., Kennedy, B.J., et al., *Ber. Bunsen-Ges. Phys. Chem.*, 1990, vol. 94, p. 1014.
23. Jusys, Z., Kaiser, J., and Behm, R.J., *Electrochim. Acta*, 2002, vol. 47, p. 3693.
24. Lu, C., Rice, C., Masel, R.I., et al., *J. Phys. Chem. B*, 2002, vol. 106, p. 9581.
25. Takasu, Y., Fujiwara, T., Murakami, Y., et al., *J. Electrochem. Soc.*, 2000, vol. 147, p. 4421.
26. Takasu, Y., Itaya, H., Iwazaki, T., et al., *Chem. Commun.*, 2001, p. 341.
27. Hills, C.W., Nashner, M.S., Frenkel, A.I., et al., *Langmuir*, 1999, vol. 15, p. 690.
28. Takasu, Y., Matsuda, Y., and Toyoshima, I., *Chem. Phys. Lett.*, 1984, vol. 108, p. 384.
29. Mason, M.G., *Phys. Rev. B*: *Condens. Matter. Mater. Phys.*, 1983, vol. 27, p. 748.
30. Steigerwalt, S., Deluga, G.A., Cliffel, D.E., and Lukehart, C.M., *J. Phys. Chem. B*, 2001, vol. 105, p. 8097.
31. Joo, S.H., Choi, S.J., Oh, I., et al., *Nature*, 2001, vol. 412, p. 169.
32. Lizcano-Valbuena, W.H., Paganin, V.A., and Gonzalez, E.R., *Electrochim. Acta*, 2002, vol. 47, p. 3715.
33. Pasynskii A.A. and Eremenko I.L., *Usp. Khim.*, 1989. vol. 58, p. 303.
34. Garcia, B.L., Captain, B., Adams, R.D., et al., *J. Clust. Sci.*, 2007, vol. 18, p. 121.
35. Grosshans-Vièles, S., Croizat, J.-L., Paillaud, P., et al., *J. Clust. Sci.*, 2008, vol. 19, p. 73.
36. Grinberg, V.A., Pasynskii, A.A., Kulova, T.L., et al., *Russ. J. Electrochem.,* 2008, vol. 44, p. 187.
37. Grinberg, V.A., Pasynskii, A.A., Kulova, T.L., and Skundin, A.M., *III Ross. konf. po vodorodnoi energetike* (III Russ. Conf. on Hydrogen Power Engineering), St.-Petersburg, 2006, p. 71.
38. Grinberg, V.A., Kulova, T.L., Skundin, A.M., and Pasynskii, A.A., US Patent Application no. 20070078052, 2007.
39. Law, C.G., Grinberg, V.A., Kulova, T.L., et al., US Patent Application, no. 2007007011084, 2007.
40. Grinberg, V.A., Kulova, T.L., Maiorova, N.A., et al., *Russ. J. Electrochem.*, 2007, vol. 43, p. 75.
41. Grinberg, V.A., Emets, V.V., Mayorova, N.A., et al., *Russ. J. Coord. Chem.*, 2015, vol. 41, no. 11, p. 751.
42. Mayorova, N.A., Grinberg, V.A., Emets, V.V., et al., *Russ. J. Coord. Chem.*, 2015, vol. 41, no. 12, p. 817.
43. Paulus, U.A., Wokaum, A., Scherer, G.G., et al., *J. Phys. Chem. B*, 2002, vol. 106, p. 4181.
44. Raevskaya, V.M., Vasekin, V.V., Konobas, Yu.I., and Chemleva, T.A., *Vestnik Mos. Gos. Univ., Ser. Khim.*, 1984, vol. 25, no. 1, p. 109.
45. Cordero, B., Gómez, V., Platero-Prats, A.E., et al., *Dalton Trans.*, 2008, p. 2832.
46. Guo, J.S., Sun, G.Q., Wu, Z.M., et al., *J. Power Sources*, 2007, vol. 172, p. 666.
47. Tyumentsev, M.S., Shiryaev, A.A., Zubavichus, Ya.V., and Anan'ev, A.V., *Radiochemistry*, 2014, vol. 56, no. 2, p. 150.
48. Tyumentsev, M.S., Anan'ev, A.V., Shiryaev, A.A., et al., *Dokl. Phys. Chem.*, 2013, vol. 450, no. 2, p. 142.

Translated by Z. Svitanko